VSFORG: Visual Saliency Facilitated Optimal Region Growing For Road Region Extraction From High Resolution Satellite Images

Vijayaraja V[1], Prathusha Laxmi B[2] , Sangeetha G[3]

[1]Professor, Department of Computer Science and Engineering, KL University,
[2]Associate Professor, Department of Information Technology, R.M.K College of Engineering,
[3]Assistant professor, Department of Information Technology, Sri Venkateswara College of Engineering,

Abstract

In obvious, the objective is to improve the performance of visual saliency aided optimal region growing for road region extraction from high spatial resolution multispectral satellite images. Satellite and aerial images are the most important available data sources for map generation and updating of available maps and they have highly improved in terms of spatial, spectral and temporal resolutions. In the proposed model satellite images is extracted using feature extraction such as color, intensity and orientation. Image transformation through Lifting Wavelet Transformation (LWT) is make use of three feature extractions then the image interpolation using bi cubic method is used for resize the extracted images and after applying this bi-cubic method the saliency map is located. The visual saliency Facilitated aided optimal region growing (VSFORG) is used for road region segmentation. In this segmentation different optimization techniques is applied for threshold optimization. In the result various evaluation metrics is analyzed mainly the accuracy for GWO is 82%, for ABC is 74% and for PSO is 64%. The proposed model is performed high when compared with other algorithms in the threshold optimization process.

Keyword: *Lifting Wavelet Transform (LWT), Feature Extraction, Satellite images, Optimal Region Growing (ORG) and Grey Wolf Optimization (GWO)*

1. Introduction

Recently road extraction from satellite imagery has emerged as one of the hot topics in the research field. It is particularly employed in the city planning, cartography and to revise already detected roads in Geographic Information Systems (GIS) environment [1]. Road extraction is a crucial aspect for the resourceful utilization of high resolution satellite images. Some of the several applications of road extraction are renewal of GIS database, reference for image registration, assistance for identification algorithms and fast mapping [2]. Road extraction enables the road network to be truly presented in the object space when the image to ground systems transformation is carried out and it has been described as the method of detection and precise localization of roads in the image [3]. Automatic road extraction attempts to simplify and speed up the road extraction process by focusing on automating all or few parts of this process. Spatial data capturing and updating for GIS applications give prime importance to road extraction from high resolution imagery [4]. Road network information is required for a variety of applications. Such information is a necessary input to many decision processes. Manual extraction of road from remote sensing (RS) imagery is mostly time-consuming and costly [5]. Moreover, tracking of road edge points in the presence of noise is the most difficult problem in road extraction because edge points along the road are not necessarily connected in the original edge map [6].

Information about road intersections or junctions is of high importance in understanding road network topologies. In [7], junction hints are used in the network optimization process by forcing roads to pass through detected T- and L-shaped junctions. Roads in satellite imagery tend to have uniform features that are distinct from neighboring regions, it is reasonable to expect that they can be automatically extracted using Gestalt grouping principles.

In the past few years, a feast of novel techniques has been given the green signal to successfully address the recognition of roads from the satellite images. Standing out amongst them are the knowledge based techniques, mathematical morphology [8], [9], [10], snakes [11], [12], classification [13], differential geometry [14], region competition [15], active testing [16], perceptual grouping [17], and the dynamic programming [18]. Further, the representative work under the Bayesian structure may be broadly categorized into two types as detailed below. (a) The state evaluation for the linear and Gaussian model employing the Kalman filter and its variants like the fragrance-free Kalman filter and comprehensive Kalman filter. (b) the state evaluation for the non-linear and Non-Gaussian challenge by deploying the Sequential Monte Carlo approaches [19] otherwise termed as the Condensation filter [20], Bootstrap filter [21], and the particle filter [22], [23]. The sterling merits of the Sequential Monte Carlo approaches (Particle filter) involve the scaling down of the sampling patches in the course of the tracking and its incredible skills of effectively addressing multi modal distribution created by cluttered scenario. The advancement or augmentation of the semiautomatic methods is highly essential to facilitate the quick, reliable and accurate furnishing of the data for the GIS techniques like the complete, or just approximately complete, mechanized procedures which have not failed to turn the corner and become sufficiently mature [24].

In this paper, we propose a metaheuristic approach based on Grey Wolf Optimization (GWO) to identify the potential positions and segment the road region using VSORG.

Our main contributions are summarized as follows:

- We present a GWO based approach for segmentation of visual saliency optimal road region.
- We present an efficient scheme for population representation.
- We derive an efficient fitness function and separate the solution based on the fitness.
- We update the position in the algorithm.
- We perform extensive simulation on the proposed algorithm, compare and analyze results with existing and related algorithms.

The remainder of this paper is organized as follows. Section 2 illustrates review of related works, section 3 provides proposed visual saliency based optimal region growing for road region extraction algorithm, section 4 provides result and discussion finally in section 5 illustrates the conclusion.

2. Review of Related works

In the literature survey, several methods have been proposed for the road extraction. Among the most recently published works are those presented as follows: Chu He *et al.* [25] have explained the Road Extraction from SAR Imagery Based on Multi-scale Geometric Analysis of Detector Responses. Before running the algorithm, a response map made up of responses, which was binarized, skeletonized, and vectorized to generate road candidates, was obtained by applying a local detector to a SAR image first. Then the method identifies real road segments among the candidates and fills gaps between them. It works in three steps. 1) Guidance segments were extracted at different resolutions from the response map using multi-scale techniques and merged to get a more appropriate approximation. 2) Segments were labeled "road" or "noise" using relaxation labeling techniques, among which "road" ones were grouped as they may lie on different roads. 3) Connection points between candidates were acquired by mapping candidates to grouped "road" guidance segments. Those connection points were linked with straight lines or curvilinear segments after a segmentation process.

Moreover, Aluir *et al.* [26] have explained the Object-Space Road Extraction in Rural Areas Using Stereoscopic Aerial Images. A strategy based on the dynamic programming algorithm provides a solution to the road extraction problem in the object space. The direct tracing of road centerlines in the object space necessitates mathematical relationships connecting road points in the stereoscopic image spaces and in the object space, enabling integration of radiometric information from the stereoscopic images into the associated energy function. The extraction process begins by first measuring a few seed points in one image of the stereoscopic pair and then transforming these into the object-space reference system. Experimental results were showed that the method was efficient and usually provided accurate road centerlines.

Similarly, Zelang Miao *et al.* [27] have explained the Road Centerline Extraction from High-Resolution Imagery Based on Shape Features and Multivariate Adaptive Regression Splines. Road centerline extraction from remotely sensed imagery was used to update a Geographic Information System (GIS) database. The common road extraction from high-resolution imagery was based on spectral information only; it was difficult to separate road features from background completely, and a thinning algorithm always results in short spurs which reduce the smoothness of the road centerline. To overcome the aforementioned shortcomings of the common existing road centerline algorithms, this method to extract the road centerline from high-resolution imagery based on shape features and multivariate adaptive regression splines (MARS), in which potential road segments were obtained based on shape features and spectral feature, followed by MARS to extract road centerlines.

In [28], Jenita Subash and Madhan Kumar have explained the Road Tracking from High resolution IRS and IKONOS Images Using Unscented Kalman Filtering. UKF was used for tracing the median axis of the single road segment. The Extended Kalman Filter (EKF) was probably the most widely used estimation algorithm for road tracking. However, more than 35 years of experience in the estimation community has shown that was difficult to implement and is difficult to tune. To overcome this limitation, UKF was introduced in road tracking which was more accurate, easier to implement, and uses the same order of calculations as linearization. The principles and algorithm of EKF and UKF were also discussed. The core of our system was based on profile matching. UKF traces the road beyond obstacles and tries to find the continuation of the road finding all road branches initializing at the road junction. The completeness and correctness of road tracking from the IRS and IKONOS images were also compared.

Additionally, K. Madhan Kumar and R. Kanthavel [29] have explained the Road Extraction from Satellite Images Using Unscented Kalman Filter and Gauss-Hermite Kalman Filter. Here, Unscented Kalman filter (UKF) was used in combination with Gauss-Hermite Kalman Filter (GHKF) to trace and identify various connected road paths and to avoid obstacles under diverse conditions. Unscented Kalman filter (UKF) component was responsible for tracing axis coordinates of a road region until it comes to a severe obstacle or an intersection. Then, the Gauss-Hermite Kalman Filter (GHKF) module takes the control of the road extraction process and regains track of the road or possibly road branches on the other side of a road junction or obstacle. From the results, they ensure that the road extraction technique outperformed the existing approach by achieving the accuracy of 98.452% in cluster 10.

Moreover, Zelang Miao *et al.* [30] have explained the Semi-Automatic Method for Road Centerline Extraction from VHR Images. This method consists of three main steps. First, the geodesic method was used to extract the initial road segments that link the road seed points prescribed in advance by users. Next, a road probability map was produced based on these coarse road segments and a further direct thresholding operation separates the image into two classes of surfaces: the road and non-road classes. Using the road class image, a kernel density estimation map was generated, upon which the geodesic method was used once again to link the foregoing road seed points. Experiments demonstrate that this proposed method was extract smooth correct road centerlines.
Now-a-days, satellite and aerial images are the most important available data sources for map generation and updating of available maps and they have highly improved in terms of spatial, spectral and temporal resolutions. Research communities are overwhelmed by the sheer volume of collected images, the necessity of automatic generation of road map and map updating seems to be very important. Due to its difficulty of extracting the road map automatically, many researchers have been carried out in this area with human intervention. In accordance with this, for road-extraction from satellite images, numerous significant algorithms and methods are published in this area. Most of the algorithms suggested in literature for road extraction consist of one or more of the following operations: image segmentation, detection of a pair of parallel linear segments, active contours, morphological operations for cleaning and bridging discontinuities, matching of road templates, etc. However, the complete automation of the road extraction processes is still a hard problem which has not been solved with a reasonable degree of success (accuracy) over a large set of images of different categories of urban and suburban areas. [30,31].

3. Proposed Visual Saliency based Optimal Region Growing for Road Region Extraction Algorithm

The main intention of the work is to improve the performance of visual saliency aided optimal region growing (VSAORG) for road region extraction from high spatial resolution multispectral satellite images. Satellite and aerial images are the most important available data sources for map generation and updating of available maps and they have highly improved in terms of spatial, spectral and temporal resolutions. In our proposed work, the satellite images is utilized for finding segmented saliency maps different process is performed. In the feature extraction stage, three types of features like intensity, color and orientation will be extracted. Before extraction the image transformation through Lifting Wavelet Transformation (LWT) is employed for three features. Then the image interpolation using bi-cubic method is utilized for resizing the images. After that, a fusion scheme based saliency map will be constructed to extract the road area from the remote sensing image.

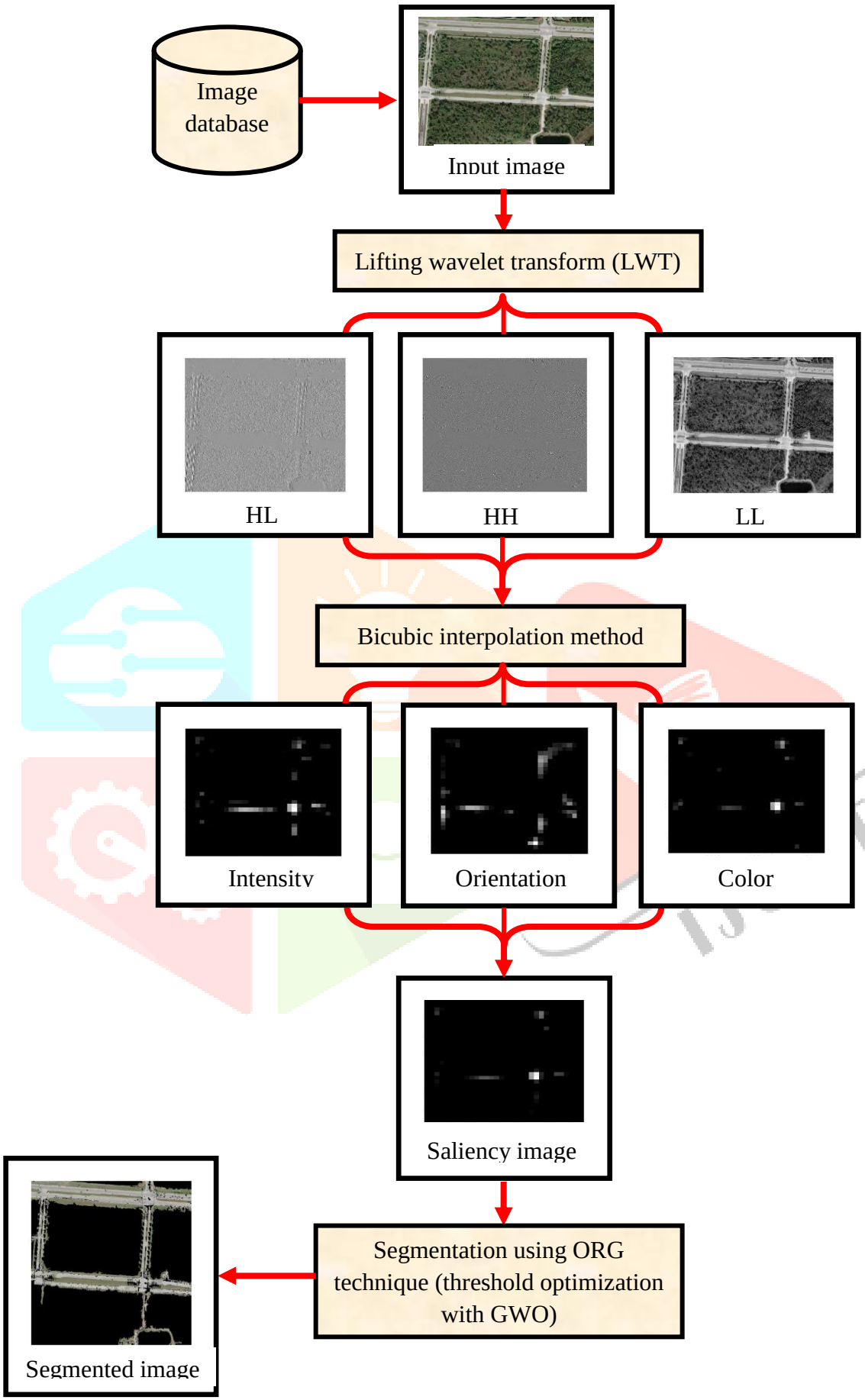

Figure.1: Framework of the proposed model

The optimal region growing technique is used to segment the image it will be implemented using MATLAB and then, for threshold optimization the performance of the algorithm will be analyzed using evaluation metric (accuracy) with various parameters. The flowchart for overall process is shown in figure 1.

3.1 Image transformation through Lifting Wavelet Transformation

The lifting wavelet transform (LWT) has been widely used in image procession. The lifting wavelet transform decomposes images into low-frequency sub-bands that reserve most of the information in the original images and high-frequency sub bands that indicate the texture and edges. The vital causes for the increasing enthusiasm in this regard may be stated as follows.

(a) The ease or convenience of the technique.
(b) The less computational complexity associated with the algorithm
(c) The skills to evaluate the signal in diverse frequency bands related to the diverse signal features.

In this regard, wavelet thresholding, or shrinkage emerges as the most well-known wavelet-based de-noising technique, which disintegrates the observed signals into sub-bands and the noise is filtered by eliminating the coefficients which are smaller than a group of specified thresholds. Habitually, a lifting scheme flows through the following three vital phases such as the split, predict and update which are detailed in the following section.

Split

It is otherwise known as the lazy wavelet transform. Here, the input image I_f is segmented into two samples such as the even sample $I_g[n]$ and odd sample $I_h[n]$: $I_g[n]$ and $I_h[n]$, and is represented as per the following Equation 1

$$Split\ I_f = \left[even(I_f), odd\ (I_f)\right] \quad (1)$$

Predict

It is predominantly a high pass filtering function, in which the odd samples $I_h[n]$ are predicted by employing the even samples $I_g[n]$ and the abstract difference $A[n]$ is evaluated as per Equation 2 shown below.

$$A[n] = I_h[n] - B\left(I_g[n]\right) \quad (2)$$

Where;

$B[\cdot]$ → Prediction operator

The high frequency component $A[n]$ is represented by the error between the original sample and its predicted value. The Prediction operator $B[\cdot]$ is a linear integration of the neighboring even coefficient for each $I_h[n]$, and B is characterized as per Equation (3) given hereunder.

$$B\left(I_g[n]\right) = \sum_{i=1}^{N} B_i\ I_g[n+1] \quad (3)$$

Where;

N → Number of point will attend the weighting prediction

B_i → Set of weighting factors of one wavelet coefficient

Update

In this updation step, scaling coefficient (approximation coefficient) $c[n]$ is produced by combining $I_g[n]$ and $U(A[n])$.

$$c[n] = I_g[n] + U(A[n]) \quad (4)$$

Where;

$I_g[n]$ → Even indexed point

$U(A[n])$ → Linear combination

The $U(A[n])$ is can be defined as follows;

$$U(A[n]) = \sum_{i=1}^{N'} u_i A[n+i] \quad (5)$$

Where;

N' → Number of wavelet coefficient points will attend the weighting update.

u_i → Lifting factor

Here, $U(A[n])$ determine the properties of the primal wavelet and dual scaling function. A construction of the ***Deslauriers– Dubuc*** family of wavelets can be seen as (6) and (7).

$$A[n] = I_g[n] - \left(\begin{matrix} I_g[n-1] + 9I_g[n] + \\ 9I_g[n+1] + I_g[n+2] \end{matrix} \right) \Big/ 16 \quad (6)$$

$$c[n] = I_g[n] + \left(\begin{matrix} A[n-2] + 9A[n-1] + \\ 9A[n] + A[n+1] \end{matrix} \right) \Big/ 32 \quad (7)$$

The Predict step has the effect of cancelling cubic polynomials, leaving the left over in the high-pass signal $A[n]$. The Update step paves the way for a low passed and sub-sampled edition of $I_f[n]$ being positioned in $c[n]$. Figure 2 effectively illustrates the procedure of the forward lifting technique.

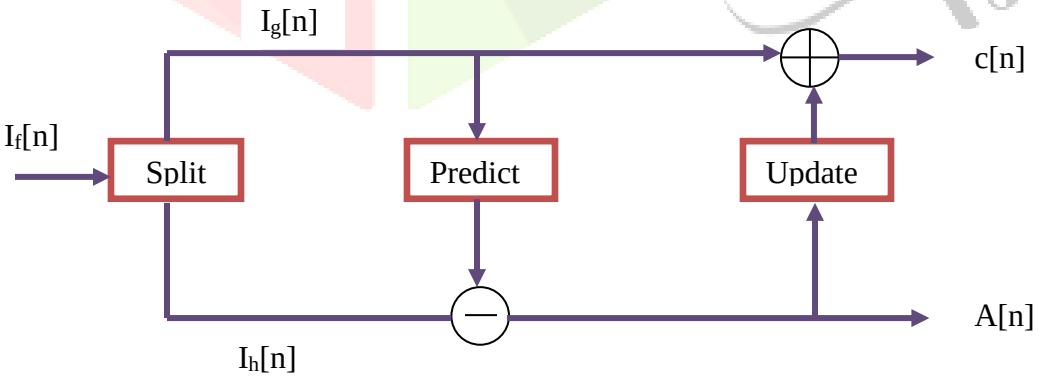

Figure.2: The forward lifting scheme

In this paper, the LWT of an image V is denoted by U and is assumed in the different scales to be of the form:

$$U = \left\{ u^1, u^2, \ldots, u^p, v^p \right\} \quad (8)$$

Here, v^p represent the approximation or low frequency bands at the last decomposition level; u^p represent the details or high frequency sub-bands at level p.

Here, u^p is composed of twelve directional sub-bands, six of which are real, and six are imaginary:

$$u^p = \begin{cases} real & u^p_{real}(x,y|1), u^p_{real}(x,y|2), \ldots, u^p_{real}(x,y|6) \\ imaginary & u^p_{imag}(x,y|1), u^p_{imag}(x,y|2), \ldots, u^p_{imag}(x,y|6) \end{cases} \quad (9)$$

Here, we use the coordinates (x,y) or the shorthand notation of $(.)$, to index the spatial position of the coefficients.

3.2 Image interpolation using Bi-cubic method

Bi-cubic interpolation is an extension of cubic interpolation for interpolating data points on a two dimensional regular grid. The interpolated surface is smoother than corresponding surfaces obtained by bilinear interpolation or nearest-neighbour interpolation. Bi-cubic interpolation can be accomplished using Lagrange polynomials, cubic splines, or cubic convolution algorithm.

In image processing, bi-cubic interpolation is often chosen over bilinear interpolation or nearest neighbour in image resampling, when speed is not an issue. In contrast to bilinear interpolation, which only takes 4 pixels (2×2) into account, bi-cubic interpolation considers 16 pixels (4×4). Images resampled with bi-cubic interpolation are smoother and have fewer interpolation artifacts.

The interpolated surface is written as

$$P(u,v) = \sum_{i=0}^{3}\sum_{j=0}^{3} a_{ij} u^i v^i \quad (10)$$

Bi-cubic interpolation on an arbitrarily sized regular grid can then be accomplished by patching together such bi-cubic surfaces, ensuring that the derivatives match on the boundaries.

By using this bi-cubic interpolation method the image will be scaled then the intensity, orientation and colour is analyzed and the saliency map is predicted. After that segmentation process is carried out named as modified region growing technique it is used for segmenting the images which has been explained below.

3.3 Feature Extraction

In the feature extraction there are three categories namely orientation, intensity and color are explained below:

3.3.1 Orientation feature extraction based LWT

The multi-scale orientation feature maps are generated using ann-level LWT, as follows:

$$[A_\sigma, H_\sigma, V_\sigma, D_\sigma] = LWT\ (A_{\sigma-1}) \qquad \sigma = 1,2,3,....n, \tag{11}$$

$$n = [(\log_2 l)/2], \tag{12}$$

Where, $A_\sigma, H_\sigma, V_\sigma$ *and* D_σ are the approximation component and the horizontal, vertical and diagonal detail coefficients, respectively. A_0 denotes the input image, and l is the size of the input image.

3.3.2 Intensity feature extraction based on logarithm co-occurrence histogram

Visual saliency, which is often perceived by global ‘‘uncommonness” and local ‘‘discontinuity” with respect to the surroundings, can therefore be determined based on the low-frequency pixel occurrence and co-occurrence information. Different from the traditional image histogram that only counts the occurrence of gray value; the co-occurrence histogram (CH) is able to concurrently calculate both global pixel occurrence and local co-occurrence of pixel pairs within a neighbourhood window. Hence it can serve as a good tool to capture both local and global saliency information for ROI detection. A typical co-occurrence histogram (denoted as CH) is obtained as follows:

$$CH = [\ ch\ (m,n)], m,n \in \{1,2,....256\}, \tag{13}$$

Where, CH is a 256*256 matrix. The element $ch\ (m,n)$ is relative to a central pixel with a gray value of m and a surrounding pixel with a gray value of n within a square neighbourhood window of size l.

3.3.3 Color feature extraction based on color opponency

Color feature is processed according to the so-called color opponent mechanism. Such opponency exists for the red-green (R-G), green-red (G-R), blue-yellow (B-Y), and yellow-blue (Y-B) color contrast channels in the HSV. For remote sensing images, color information corresponds to spectral bands in multi-spectral images. These bands are not always in one-to-one correspondence with RGB channels.

3.4 Road Region Segmentation using VSORG

Region growing is a simple image segmentation method based on the region where the classification is based on the pixel-based image segmentation method since it involves the selection of initial seed points. This approach to segmentation examines the neighbouring pixels of initial “seed points” and determines whether the pixel neighbours have to be added to the region or not based on certain conditions. The process is iterated to yield different regions in an original region growing. The normal region growing has the drawback of variation of intensity that may result in holes or over-segmentation. For improving the original region growing and effectively tackling the drawbacks of an original region growing, we have added an additional constrain of "orientation". Here in the modified region growing, there are two thresholds, one is for the intensity and other for the orientation. Region is grown if only both constrains are met. The inclusion of this additional constrain have yielded in obtaining a much better result when compared to the original region growing.

In the original region growing method the seed point and threshold values are assigned manually for the segmentation and this does not yield better results all the time. Here in the visual saliency aided region growing, the highest intensity value attained in the histogram is assigned to be the seed point, and the threshold value is assigned manually. The optimal threshold value is predicted for the better segmentation and this will increase the accuracy of the segmented image optimization techniques that are utilized. The Grey Wolf Optimization algorithm is used to optimize the threshold and segmented the road region, thereby leading to the Optimization of the modified region growing method comprises of four steps

- Gridding
- Selection of seed point
- Threshold optimization using GWO
- Applying region growing to the point

3.4.1 Gridding

In gridding, a single image is divided into several smaller images by drawing an imaginary grid over it. That is, gridding results in converting the image into several smaller grid images. The grids are usually square in shape and the grid number to which the original image is split into is a variable.

At first, the image is divided into numerous blocks (O_s), and as it resembles applying a grid on the image, this process is identified as gridding. The gridding is done to allocate each spot with individual compartments.

3.4.2 Selection of seed point

In this process, the histogram evaluation is employed to usher in the seed point. The histogram is found out for every pixel in the grid. As the image is a grey scale image, the values of this image is from 0 to 255. For every grid, the histogram value that comes most frequent is selected as the seed point pixel. From this, any one of the seed point pixel is taken as the seed point for the grid.

$$block(u,v) = k_u(y:(y+O_s)-1, l:(l+O_s)-1) \qquad for\ (u=1.....10):r \quad (v=1.....10):c \qquad (14)$$

$$[Oy_{uv}\ Ol_{uv}] = find(block\{u,v\} == \max(block\{u,v\})) \qquad (15)$$

$$y = y + O_s, \quad l = l + O_s$$

After finding out the seed point, the region is grown from it. Here the neighbouring pixels are compared with the seed point and if the neighbour pixel satisfies constrains, then the region is grown else it is not grown to that pixel. Constrains for our proposed region growing is the “intensity” and the “orientation”. In a normal region growing, only the intensity constrain is taken into account. For the intensity constraint, an intensity threshold is also set in-order to check if the neighbour pixel satisfies the condition. Intensity threshold defines the maximum value by the neighbour pixel value can differ from the pixel in consideration. Suppose the pixel is having the intensity value I_R , and the neighbouring pixel has the value I_S and the intensity threshold is set as T_I , then if $\| I_R - I_S \| \le T_I, then$ intensity constrain is met and satisfied.

In-order to find the "orientation" constraint, first the gradients in x and y axis are found out and calculate according to the formula given below. Let I_x be image values after applying the gradient in X axis and I_y be the values after applying gradient in Y axis.

Then both the values are combined to form the gradient matrix m where $m = 1/(1+(I_x^2 + I_y^2))$. From this matrix g , we can get the orientation of each of the pixels. Suppose the pixel is having the orientation value O_R, and the neighbouring pixel has the value O_S and the orientation threshold is set as T_O , then if $\| O_R - O_S \| \leq T_O, then$ orientation constrain is met and satisfied.

When both the intensity constraint and the orientation constraint are satisfied by a neighbouring pixel, then the region is grown to the neighbour pixel and the region grows.

That is if $\| I_R - I_S \| \leq T_I AND \| O_R - O_S \| \leq T_O, then$ the neighbour pixel is added to the region.

3.4.3 Threshold Optimization using GWO

This process is carried out to attain the segmented image, and for the purpose, the optimization technique is applied. In the threshold optimization the maximum accuracy is attained in the Grey Wolf Optimization (GWO) algorithm compared to the other two techniques.

3.4.3.1 Grey Wolf Optimization Algorithm

The grey wolves adequately frame a Canidae's piece family and are esteemed as the apex predators showing their position at the sustenance's food chain. They routinely show an inclination to make due as a group. The heads constitute a male and a female, labeled as alpha, which are for the most part in charge of taking suitable choices viewing different factors, for example, the hunting, sleeping place, time to wake, and so forth. The choices made by the alpha are passed on to the group. The Beta speaks to the second rank in the pecking order of the grey wolves. They are, basically, auxiliary wolves which adequately offer some assistance to the alpha in the choice making or comparable group functions.

The omega, which is at the least strata of the grey wolf pack, by and large functions as a substitute offering into the other leading wolves very nearly on each event and is permitted to have just the little scraps taking after a great blowout by the leader wolves. A wolf is marked as subordinate or as delta every so often in the event that it doesn't fit in with the gathering of an alpha, beta, or omega. In spite of the fact that these delta wolves need to respect the alphas and betas, they, then again, have a successful predominance over the omegas. In our technique, the alpha (α) is esteemed as the most suitable arrangement with a perspective to replicating logically the social pecking order of wolves while conceiving the GWO. Thus, the second and the third best arrangements are named as beta (β) and delta (δ) separately. The remaining applicant arrangements are regarded to be the omega (ω). In the GWO method the hunting (optimization) is guided by the α , β , δ and ω . [32, 33].

Initialization process

In the district developing procedure, we pick the seed point and the centroid fragment the image. Here we introduce the centroid c_i and certain algorithm parameters, for example, $a, G, and\ L$ as coefficient vectors.

Fitness evaluation

In every square of the image we continue to find the fitness F_i in a portioned part and here the fitness is the most extreme precision of the fragmented part.

Separate the solution based on the fitness

Now, we find the separate solution (threshold) based on the fitness value. Let the first best fitness solutions be α, the second best fitness solutions β and the third best fitness solutions δ.

Update the position

We assume that the alpha (best candidate solution), beta and delta have the improved knowledge about the potential location of the prey in order to reproduce mathematically the hunting behavior of the grey wolves. As a result, we hoard the first three best solutions attained so far and require the other search agents (including the omegas) to revise their positions according to the position of the best search agent. For repetition, the new solution $k(t+1)$ is estimated by using the formulae mentioned below.

$$H^{\alpha} = | K_1.k_{\alpha} - k |, \quad H^{\beta} = | K_2.k_{\beta} - k |, \quad H^{\delta} = | K_3.k_{\delta} - k |) \tag{16}$$

$$k_1 = k_{\alpha} - G_1.(H_{\alpha}), k_2 = k_{\beta} - G_2.(H_{\beta}), \quad k_3 = k_{\delta} - G_3.(H_{\delta}) \tag{17}$$

To have hyper-spheres with different random radii, the arbitrary parameters G and k help the candidate solutions. Examination and usage are ensured by the adaptive estimations of G and a .The adaptive estimations of the parameters G and a license the GWO to travel them easily among the investigation and the usage. With diminishing G, half of the iterations are committed to the investigation ($|G|<1$) and the other half are dedicated to the usage. Enclosing the conduct, the subsequent equations are utilized keeping in mind the end goal to give numerical model.

$$H = | K.k_P(t) - k(t) | \tag{18}$$

The coefficient vectors are found by the equation (19)

$$G = 2a.r_1 - a, \qquad K = 2.r_2 \tag{19}$$

Where t indicates the current iteration, G and K are coefficient vectors, k_P is the position vector of the prey c and indicates the position vector of a grey wolf. The components of a are linearly decreased from 2 to 0 over the course of iterations and r_1, r_2 are random vectors in [0, 1].

The GWO has only two main parameters (G and K) to be adjusted. However, we have kept the GWO algorithm as simple as possible with the fewest operators to be adjusted. The process will be continued until the maximum accuracy is obtained.

4. Result and discussion

In this section the result is discussed based on satellite image datasets. For finding segmented saliency maps various feature extractions is utilized namely colour, intensity and orientation. The Lifting Wavelet Transformation (LWT) applied for intensity and orientation. After image transformation interpolation method as bi-cubic is used for scaling then the saliency maps is predicted and the segmentation is performed in the saliency maps. In the segmentation process threshold optimization technique with Grey Wolf Optimization (GWO) algorithm is performed and find the Accuracy, Sensitivity, Specificity, True Positive (TP), True Negative (TN), False Positive (FP), False Negative (FN), Positive Predictive Value (PPV), Negative Predicted Value (NPV), False Positive Rate (FPR), False Discovery Rate (FDR), Sensitivity and Specificity/2, Random Index (RI), Global Consistency Error (GCE) and Variation of Information (VI). Below figure 3 shows input data for extraction.

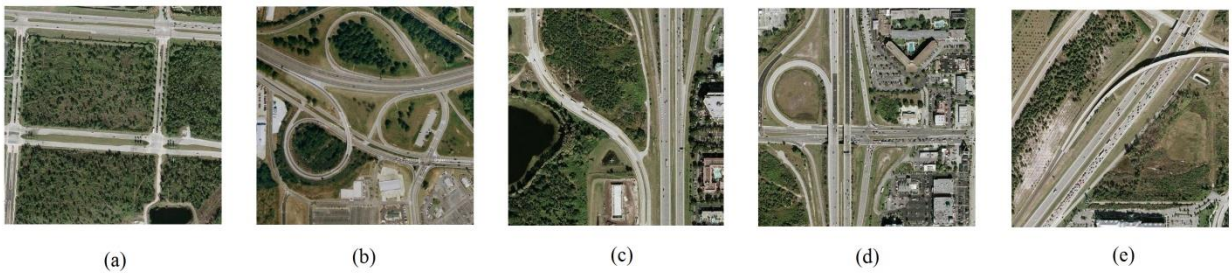

Figure.3: Input data

Table.1: overall result for proposed algorithm

Input image	Feature extractions	Saliency map	Segmented image
a.	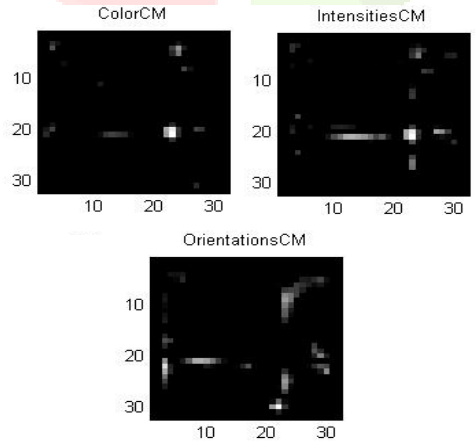	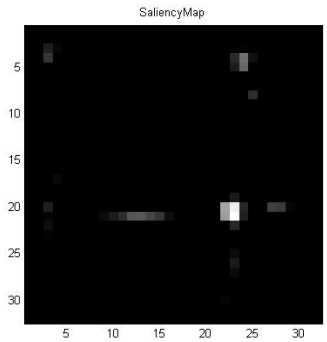	

b.	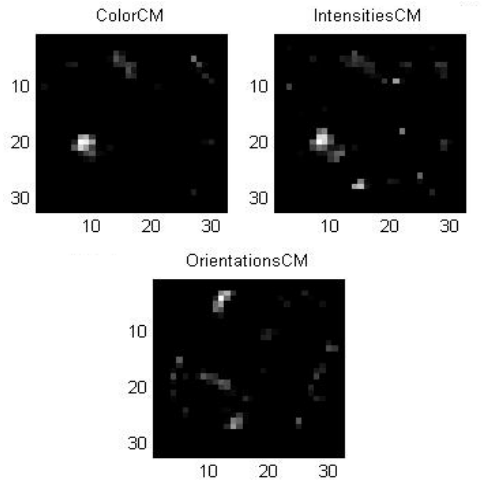 ColorCM IntensitiesCM OrientationsCM	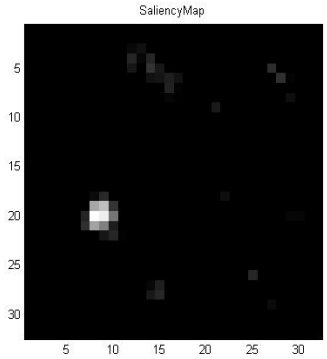 SaliencyMap	
c.	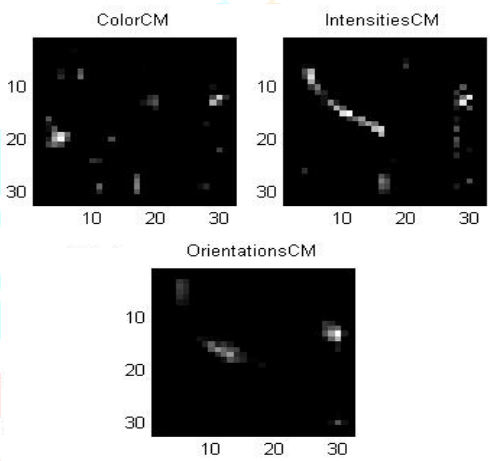 ColorCM IntensitiesCM OrientationsCM	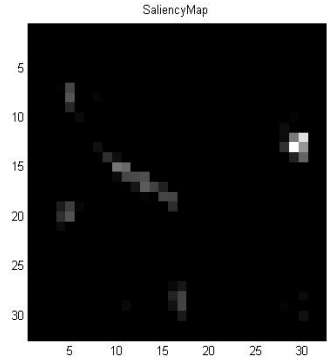 SaliencyMap	
d.	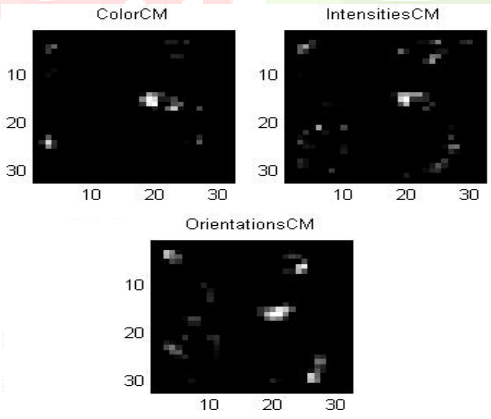 ColorCM IntensitiesCM OrientationsCM	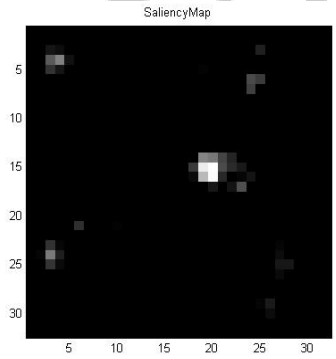 SaliencyMap	

e.	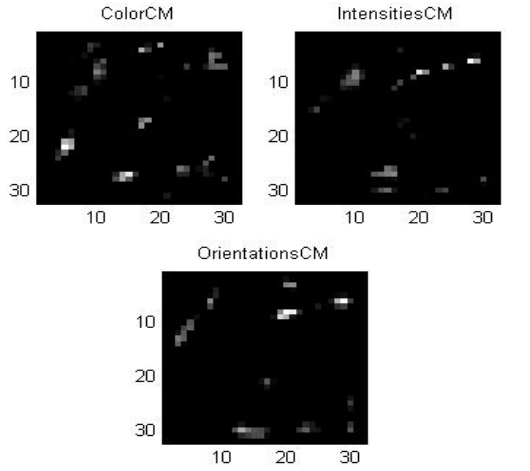	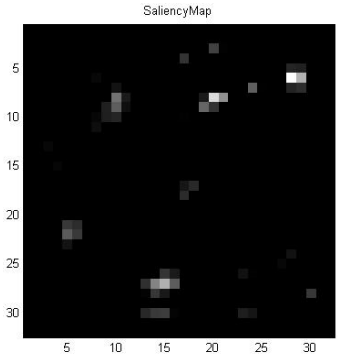	

Table 1 has been shows that the input image, feature extractions namely color, intensity and orientation images, saliency maps and segmented images for proposed (GWO) algorithm.

Table.2: performance analysis of proposed algorithm for satellite images

Image name	TP	TN	FP	FN	Sen	Spec	Acc	PPV	NPV	FPR	FDR	Sen+ Spec/ 2	RI	GCE	VI
a	57410	172656	15628	16450	0.777	0.916	0.877	0.786	0.913	0.083	0.213	0.847	0.785	0.206	1.028
b	103930	113137	21078	23999	0.812	0.842	0.828	0.831	0.824	0.157	0.168	0.827	0.715	0.284	1.323
c	56788	155106	4292	45958	0.552	0.973	0.808	0.929	0.771	0.026	0.070	0.762	0.690	0.225	1.177
d	119595	80282	8751	53516	0.690	0.901	0.762	0.931	0.600	0.098	0.068	0.796	0.637	0.307	1.417
e	53599	163940	30672	13933	0.793	0.842	0.829	0.636	0.921	0.157	0.363	0.818	0.717	0.246	1.228

Table 2 shows the performance analysis of proposed (GWO) algorithm for satellite images. The evaluation of saliency map in different images is carried out by applying the following equations.

Sensitivity: Sensitivity is a measure which determines the probability of the results that are true positive as 'that region as road'.

$$Sensitivity = \frac{Number\ \text{of True Positives}}{\text{Number of True Positives} + \text{Number of False Negatives}} \quad (20)$$

Specificity: Specificity is a measure which determines the probability of the results that are true negative as 'that region is not road'.

$$Specificity = \frac{Number\ \text{of True Negatives}}{\text{Number of True Negatives} + \text{Number of False Positives}} \quad (21)$$

Accuracy: Accuracy is a measure which determines the probability that how may results are accurately classified.

$$Accuracy = \frac{(\text{TP} + \text{TN})}{\text{TP} + \text{TN} + \text{FP} + \text{FN}} \quad (22)$$

Positive and Negative Predictive Values (PPV) and (NPV): PPV and NPV indicate the fraction of positive outcomes and negative outcomes in statistics with diagnostic tests in order. They are, correspondingly, called the results true positive and true negative.

$$Positive\ \text{Predictive Value}(PPV) = \frac{TP}{(TP + FP)} \quad (23)$$

$$\text{Negative Predictive Value}(NPV) = \frac{TN}{(TN + FN)} \quad (24)$$

False Positive Rate (FPR): FPR offers the fraction of individuals, who were wrongly categorized as positive, but actually belong to negative classification.

$$False\ Positive\ Rate\ (FPR) = \frac{\text{FP}}{\text{N}} = \frac{FP}{(FP + TN)} \quad (25)$$

False Discovery Rate (FDR): FDR control refers to a statistical approach, which is used in multiple hypothesis testing to attain precise multiple comparisons.

$$False\ \text{Discovery}\ Rate\ (FDR) = \frac{FP}{(FP + TP)} \quad (26)$$

Random Index (RI): Rand index calculates the fraction of pairs of pixels labeling that they become steady between the computed segmentation and the ground truth. The Rand index or Rand measure is a calculation of the similarity between the two clusters.

$$RI = \frac{a + b}{a + b + c + d} \quad (27)$$

Where, a + b is the number of agreements between the partitions X and Y and c + d is the number of disagreements between the partitions X and Y.

Global Consistency Error (GCE): GCE measures the extent to which segmentation can be viewed as a refinement of the other. Segmentation is simply a division of the pixels of an image into sets.

$$GCE = \frac{1}{n}\min\left\{\sum_i E(S_1.S_2, p_i), \sum_i E(S_2.S_1, p_i)\right\} \quad (28)$$

Where segmentation error measure takes two segmentations S1 and S2 as input, these values contain pixel.

Variation of Information (VOI): The VOI metric defines the distance between the two segmentations as average conditional entropy of one segmentation to the other.

$$VI(X;Y) = H(X) + H(Y) - 2I(X,Y) \quad (29)$$

Where, H(X) is entropy of X and I(X, Y) is mutual information between X and Y.

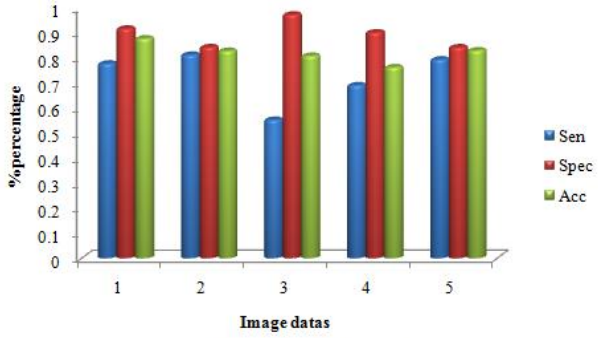

(a) For GWO algorithm

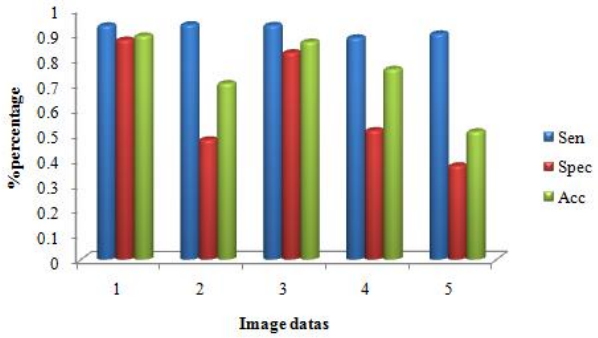

(b) For ABC algorithm

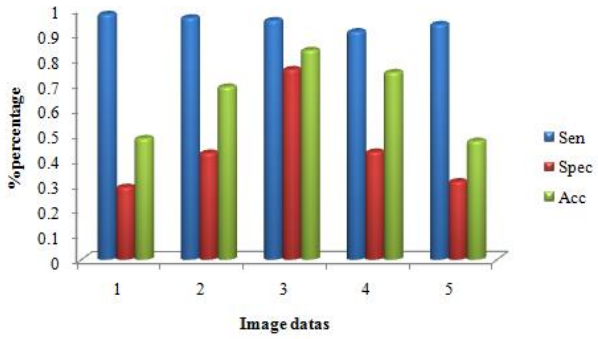

(c) For PSO algorithm

Figure.4: performance graph for GWO, ABC and PSO algorithms

In figure 4 the performance graph for GWO, ABC and PSO algorithm of sensitivity, specificity and accuracy is shown above. Each figure (a), (b) and (c) is denoted the three algorithms for 5 images the evaluation metrics is analyzed.

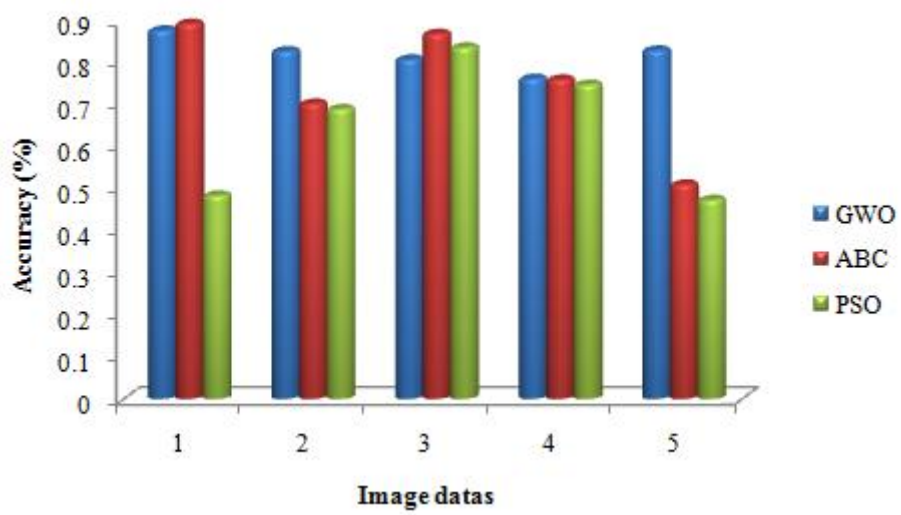

Figure.5: Accuracy graph for three algorithms

Above figure 5 shows the accuracy for GWO, ABC and PSO algorithms. In this graph, 5 satellite image datasets is used and accuracy varies 0 to 0.9. For ABC algorithm the accuracy value for image 1 is 0.89%, image 2 is 0.70%, image 3 is 0.869%, image 4 is 0.76% and image 5 is 0.51%. For PSO algorithm the accuracy value for image 1 is 0.48%, image 2 is 0.69%, image 3 is 0.83%, image 4 is 0.74% and image 5 is 0.47%. Finally, in GWO algorithm the accuracy value for image 1 is 0.87%, image 2 is 0.82%, image 3 is 0.808%, image 4 is 0.76% and image 5 is 0.82%. From this graph the GWO algorithm is performed better it has high accuracy level.

5. Conclusion

In the conclusion part satellite image extraction is discovered using transformation images as (LWT), feature extraction as color, intensity and orientation, interpolation method, saliency maps, optimal region growing techniques with GWO algorithm for segmentation process. Based on these techniques various evaluation metrics is analyzed namely Accuracy, Sensitivity, Specificity, TP, TN, FP, FN, PPV, NPV, FPR, FDR, Sensitivity and Specificity/2, RI, GCE and VI. For ABC algorithm the accuracy value is 74% and for PSO algorithm the accuracy value is 64%. The accuracy of proposed model (GWO) value is 82% which was higher than other techniques. In future various feature extraction, optimization techniques and comparisons are to be used for enhanced performance.

Reference

[1] Saurav Jyothi, Dhruba K.Bhattacharya, "A Grid Density Based Technique for Finding Clusters in Satellite Images", Elsevier Pattern Recognition Letters, May 2011.

[2] P.N.Anil, Rizvi and B.Krishna Mohanam, "Object-Oriented Method for Automatic Extraction of Road from High Resolution Satellite Images", Iranian Journal of Earth Science, 2010.

[3] F.Benkoudier, L.Hamam and A.Abdellaoui, "Use of Neural Net for Road Extraction from Satellite Images", Progress in Electromagnetic Research symposium Proceedings, March 2011.

[4] D.Chaudri, N.K.Kushwaha and A.Samal, "Semi Automated Road Detection From High Resolution Satellite Images by Direction Morphological Enhancement And Segmentation Techniques", IEEE Journal of Selected Topics in Applied Earth Observations and Remote Sensing, October 2012.

[5] Hesamodin dehghaniana, Mohamad Javad ValadanZouja, Hamid Ebadia and Mehdi Mokhtarzadeha, "Automated Road Extraction Using Both Genetic Algorithms and Clustering Analysis from Pan-Sharpened IKONOS Images", IEEE International Geoscience and Remote Sensing Symposium, Boston, Massachusetts, U.S.A, pp. 2008

[6] Ke Qifa, Xiao Jing, Yang Zhiyong and Songde Ma, "Energy-based Method for Road Extraction from Satellite Images",IAPR Workshop on Machine Vision Applications, Tokyo, Japan, 1996.

[7] M. Negri, P. Gamba, G. Lisini, and F. Tupin, "Junction-aware extraction and regularization of urban road networks in high-resolution SAR images, "IEEE Transaction Geoscience Remote Sensing, vol. 44, no. 10, pp. 2962–2971, Oct. 2006.

[8] F. Tupin, H. Maitre, J. F. Mangin, J. M. Nicolas, and E. Pechersky, "Detection of linear features in SAR images: Application to road network extraction," IEEE Trans. Geosci. Remote Sens., vol. 36, no. 2, pp. 434–453, Mar. 1998.

[9] C. Zhu, W. Shi, M. Pesaresi, L. Liu, X. Chen, and B. King, "The recognition of road network from high-resolution satellite remotely sensed data using image morphological characteristics," Int. J. Remote Sens., vol. 26, no. 24, pp. 5493–5508, Dec. 2005.

[10] A. Katartzis, H. Sahli, V. Pizurica, and J. Cornelis, "A model-based approach to the automatic extraction of linear features from airborne images", IEEE Trans. Geosci., Remote Sens., vol. 39, no. 9, pp. 2073– 2079, Sep. 2001.

[11] A. Baumgartner, C. Steger, C. Wiedemann, H. Mayer, W. Eckstein, and H. Ebner, "Update of roads in GIS from aerial imagery: Verification and multi-resolution extraction," in Proc. Int. Arch. Photogramm. Remote Sens., 1996, vol. XXXI, pp. 53–58.

[12] A. Baumgartner, S. Hinz, and C. Wiedemann, "Efficient methods and interfaces for road tracking", in Proc. Int. Soc. Photogramm., Remote Sens., 2002, pp. 28–31

[13] O. Tuncer, "Fully automatic road network extraction from satellite images," in Proc. Recent Adv. Space Technol., Jun. 2007, pp. 708–714.

[14] C. Steger, "An unbiased detector of curvilinear structures," IEEE Trans. Pattern Anal., Mach. Intell., vol. 20, no. 2, pp. 113–125, Feb. 1998.

[15] M. Amo, F. Martinez, and M. Torre, "Road extraction from aerial images using a region competition algorithm", IEEE Trans. Image Process., vol. 15, no. 5, pp. 1192–1201, May 2006

[16] D. Geman and B. Jedynak, "An active testing model for tracking roads in satellite images," IEEE Trans. Pattern Anal. Mach. Intell., vol. 18, no. 1, pp. 1–14, Jan. 1996.

[17] P. Gamba, F. Dell'Acqua, and G. Lisini,"Improving urban road extraction in high-resolution images exploiting directional filtering, perceptual grouping, and simple topological concepts", IEEE Geosci., Remote Sens. Lett., vol. 3, no. 3, pp. 387–391, Jul. 2006.

[18] M. Barzohar and D. B. Cooper, "Automatic finding of main roads in aerial images by using geometric-stochastic models and estimation," IEEE Trans. Pattern Analysis Mach. Intell., vol. 18, no. 7, pp. 707–721, Jul. 1996.

[19] A. Doucet, S. Godsill and C. Andrieu, "On sequential Monte Carlo sampling methods for Bayesian filtering", Stat. Computer, Vol.10, no. 3, pp. 197-208, 2000.

[20] Isard and Blake, "Condensation – conditional density propagation for visual tracking" International Journal of Computer Vision, pp.5–28, 1998.

[21] N. Gordon, D.Salmond and C. Ewing, "Bayesian state estimation for tracking and guidance using the bootstrap filter", Journal of gauidance , Control and Dynamics, vol. 18, no.6,pp.1434-1443,1999.

[22] Gordon, N., Arulampalam, M.S., Maskell, S., Clapp, "A tutorial on particle filters", IEEE Transaction and Signal Process, 2002.

[23] Nummiaro, K., Koller-Meier, E., Van Gool, L., "Object tracking with an adaptive colour-based particle filter" Image Vision Computer, pp.99–111, 2002.

[24] P.N.Anil, Dr.S.Natarajan, "Automatic Road Extraction from High Resolution Imagery Based on Statistical Region Merging AND skeletonisation," International journal of Engineering science and technology, May 2010.

[25] Chu He, Zi-xian Liao, Fang Yang, Xin-ping Deng, and Ming-sheng Liao, "Road Extraction From SAR Imagery Based on Multiscale Geometric Analysis of Detector Responses,"IEEE Journal Of Selected Topics In Applied Earth Observations And Remote Sensing, Vol. 5, No. 5, October 2012.

[26] Aluir P. Dal Poz, Rodrigo A. B. Gallis, João F. C. da Silva, and Érico F. O. Martins, "Object-Space Road Extraction in Rural Areas Using Stereoscopic Aerial Images", IEEE Geosciences and Remote Sensing Letters, Vol. 9, No. 4, July 2012.

[27] Zelang Miao, Wenzhong Shi, Hua Zhang, and Xinxin Wang, "Road Centerline Extraction from High-Resolution Imagery Based on Shape Features and Multivariate Adaptive Regression Splines", IEEE Geoscience and Remote Sensing Letters, Vol. 10, No. 3, May 2013.

[28] Jenita Subash and Madhan Kumar, "Road Tracking from High resolution IRS and IKONOS Images Using Unscented Kalman Filtering", International Journal of Electronic Signals and Systems, vol.1, 2014

[29] K. Madhan Kumar and R. Kanthavel, "Road Extraction from Satellite Images Using Unscented Kalman Filter and Gauss-Hermite Kalman Filter," International Review on Computers and Software (IRECOS), Vol. 8 No. 9, September 2013.

[30] Zelang Miao Bin Wang, Wenzhong Shi and Hua Zhang,"A Semi-Automatic Method for Road Centerline Extraction From VHR Images", Geoscience and Remote Sensing Letters, Vol.11 , no.11 , 2014.

[31] Sukhendu Das, T. T. Mirnalinee, and Koshy Varghese, "Use of Salient Features for the Design of a Multistage Framework to Extract Roads From High-Resolution Multispectral Satellite Images", IEEE Transactions On Geoscience And Remote Sensing, Vol. 49, no. 10, October 2011.

[32] Emary, Hossam Zawbaa and Aboul Ella Hassanien,"Binary Gray Wolf Optimization Approaches for Feature Selection",Journal of Neurocomputing, pp.1-34, 2015.

[33] Alaa Sheta and Amal Abdel-Raouf,"Estimating the Parameters of Software Reliability Growth Models Using the Grey Wolf Optimization Algorithm",Journal of advanced computer science and applications, Vol. 7, No. 4, 2016.